J|A|C|S
ARTICLES
Published on Web 02/22/2007

The Conformations of 13-Vertex $ML_2C_2B_{10}$ Metallacarboranes: Experimental and Computational Studies

Kelly J. Dalby,[†] David Ellis,[†] Stefan Erhardt,[†] Ruaraidh D. McIntosh,[†] Stuart A. Macgregor,*[,†] Karen Rae,[†] Georgina M. Rosair,[†] Volker Settels,[†] Alan J. Welch,*[,†] Bruce E. Hodson,[‡] Thomas D. McGrath,*[,‡] and F. Gordon A. Stone[‡]

Contribution from the School of Engineering and Physical Sciences, Heriot-Watt University, Edinburgh EH14 4AS, U.K., and Department of Chemistry and Biochemistry, Baylor University, Waco, Texas 76798-7348

Received October 27, 2006; E-mail: a.j.welch@hw.ac.uk

Abstract: The docosahedral metallacarboranes 4,4-$(PMe_2Ph)_2$-4,1,6-*closo*-$PtC_2B_{10}H_{12}$, 4,4-$(PMe_2Ph)_2$-4,1,10-*closo*-$PtC_2B_{10}H_{12}$, and $[N(PPh_3)_2][4,4\text{-cod-}4,1,10\text{-}closo\text{-}RhC_2B_{10}H_{12}]$ were prepared by reduction/metalation of either 1,2-*closo*-$C_2B_{10}H_{12}$ or 1,12-*closo*-$C_2B_{10}H_{12}$. All three species were fully characterized, with a particular point of interest of the latter being the conformation of the $\{ML_2\}$ fragment relative to the carborane ligand face. Comparison with conformations previously established for six other $ML_2C_2B_{10}$ species of varying heteroatom patterns (4,1,2-MC_2B_{10}, 4,1,6-MC_2B_{10}, 4,1,10-MC_2B_{10}, and 4,1,12-MC_2B_{10}) reveals clear preferences. In all cases a qualitative understanding of these was afforded by simple MO arguments applied to the model heteroarene complexes $[(PH_3)_2PtC_2B_4H_6]^{2-}$ and $[(PH_3)_2PtCB_5H_6]^{3-}$. Moreover, DFT calculations on $[(PH_3)_2PtC_2B_4H_6]^{2-}$ in its various isomeric forms approximately reproduced the observed conformations in the 4,1,2-, 4,1,6-, and 4,1,10-MC_2B_{10} species, although analogous calculations on $[(PH_3)_2PtCB_5H_6]^{3-}$ did not reproduce the conformation observed in the 4,1,12-MC_2B_{10} metallacarborane. DFT calculations on $(PH_3)_2PtC_2B_{10}H_{12}$ yielded good agreement with experimental conformations in all four isomeric cases. Apparent discrepancies between observed and computed Pt−C distances were probed by further refinement of the 4,1,2- model to 1,2-$(CH_2)_3$-4,4-$(PMe_3)_2$-4,1,2-*closo*-$PtC_2B_{10}H_{10}$. This still has a more distorted structure than measured experimentally for 1,2-$(CH_2)_3$-4,4-$(PMe_2Ph)_2$-4,1,2-*closo*-$PtC_2B_{10}H_{10}$, but the structural differences lie on a very shallow potential energy surface. For the model compound a henicosahedral transition state was located 8.3 kcal mol^{-1} above the ground-state structure, consistent with the fluxionality of 1,2-$(CH_2)_3$-4,4-$(PMe_2Ph)_2$-4,1,2-*closo*-$PtC_2B_{10}H_{10}$ in solution.

Introduction

There is significant current interest in supraicosahedral heteroborane chemistry, an area of study which began more than three decades ago with the synthesis[1] and subsequent structural study[2] of the first such species, the 13-vertex cobaltacarborane 4-Cp-4,1,6-*closo*-$CoC_2B_{10}H_{12}$. For many years large boron-based polyhedra have been of interest to computational chemists[3] and have represented a significant challenge to experimentalists. Although well over a hundred 13-vertex metallacarboranes are now known, there is still only a handful of 14-vertex species[4] and only two 15-vertex species.[5] However, recent advances,[6] including the synthesis of supraicosahedral carboranes,[7] are laying the foundations for the eventual synthesis of larger and larger heteroboranes to complement the theoretical work.

The usual structure adopted by 13-vertex metallacarboranes is the docosahedron, **I** (Chart 1). This structure (of idealized C_{2v} symmetry) has two degree-six (with respect to the polyhedron) vertices (vertices 4 and 5) and one degree-four vertex (vertex 1); all the remaining vertices are of degree-five. Recently, we have reported a variation of this basic shape.[8] In the

[†] Heriot-Watt University.
[‡] Baylor University.

(1) Dunks, G. B.; McKown, M. M.; Hawthorne, M. F. *J. Am. Chem Soc.* **1971**, *93*, 2541.
(2) Churchill, M. R.; DeBoer, B. G. *J. Chem. Soc., Chem. Commun.* **1972**, 1326.
(3) (a) Brown, L. D.; Lipscomb, W. N. *Inorg. Chem.* **1977**, *16*, 2989. (b) Bicerano, J.; Marynick, D. S.; Lipscomb, W. N. *Inorg. Chem.* **1978**, *17*, 2041. (c) Bicerano, J.; Marynick, D. S.; Lipscomb, W. N. *Inorg. Chem.* **1978**, *17*, 3443. (d) Lipscomb, W. N.; Massa, L. *Inorg. Chem.* **1992**, *31*, 2297. (e) Schleyer, P. v. R.; Najafian, K.; Mebel, A. M. *Inorg. Chem.* **1998**, *37*, 6765. (f) Balakrishnarajan, M. M.; Hoffmann, R.; Pancharatna, P. D.; Jemmis, E. D. *Inorg. Chem.* **2003**, *42*, 4650. (g) Wang, Z. X.; Schleyer, P. v. R. *J. Am. Chem. Soc.* **2003**, *125*, 10484.
(4) (a) Evans, W. J.; Hawthorne, M. F. *J. Chem. Soc., Chem. Commun.* **1974**, 38. (b) Maxwell, W. M.; Bryan, R. F.; Grimes, R. N. *J. Am. Chem. Soc.* **1977**, *99*, 4008. (c) Maxwell, W. M.; Weiss, R.; Sinn, E.; Grimes, R. N. *J. Am. Chem. Soc.* **1977**, *99*, 4016. (d) Pipal, J. R.; Grimes, R. N. *Inorg. Chem.* **1978**, *17*, 6. (e) Ellis, D.; Lopez, M. E.; McIntosh, R.; Rosair, G. M.; Welch, A. J. *Chem. Commun.* **2005**, 1917.
(5) (a) McIntosh, R. D.; Ellis, D.; Rosair, G. M.; Welch, A. J. *Angew. Chem., Int. Ed.* **2006**, *45*, 4313. (b) Deng, L.; Zhang, J.; Chan, H.-S.; Xie, Z. *Angew. Chem., Int. Ed.* **2006**, *45*, 4309.
(6) For example: (a) Ellis, D.; Lopez, M. E.; McIntosh, R.; Rosair, G. M.; Welch, A. J.; Quenardelle, R. *Chem. Commun.* **2005**, 1348. (b) Deng, L.; Chan, H.-S.; Xie, Z. *J. Am. Chem. Soc.* **2006**, *128*, 5219.
(7) (a) Burke, A.; Ellis, D.; Giles, B. T.; Hodson, B. E.; Macgregor, S. A.; Rosair, G. M.; Welch, A. J. *Angew. Chem., Int. Ed.* **2003**, *42*, 225. (b) Deng, L.; Chan, H.-S.; Xie, Z. *Angew. Chem., Int. Ed.* **2005**, *44*, 2128.
(8) McIntosh, R.; Ellis, D.; Gil-Lostes, J.; Dalby, K. J.; Rosair, G. M.; Welch, A. J. *Dalton Trans.* **2005**, 1842.

 10.1021/ja067698m CCC: $37.00

Chart 1

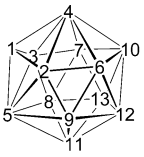

I, docosahedron

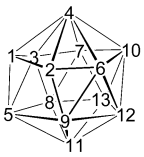

II, henicosahedron

henicosahedron, **II**, the 2−5 connectivity of the docosahedron is missing, and the structure (of idealized C_s symmetry) has a trapezoidal 1295 face.

In all known MC_2B_{10} 13-vertex metallacarboranes the metal atom occupies vertex 4, one of the positions of highest connectivity, and one carbon atom occupies vertex 1, the lowest-connected position, a simple consequence of the relative electronegativities of metals, carbon, and boron. Thus, for MC_2B_{10} species isomers are possible, based on the location of the second cage C atom. Since 13-vertex metallacarboranes are usually prepared from reduction and subsequent metalation of *closo*-C_2B_{10} carboranes, kinetic isomers of MC_2B_{10} configuration arise from the use of different carborane isomers: (i) reduction of 1,2-*closo*-C_2B_{10} carborane causes the C atoms to spontaneously separate,[9] affording [7,9-*nido*-C_2B_{10}]$^{2-}$, and metalation then affords 4,1,6-MC_2B_{10} metallacarboranes;[10] (ii) reduction of 1,7-*closo*-C_2B_{10} carborane also yields [7,9-*nido*-C_2B_{10}]$^{2-}$,[11] hence the same 4,1,6-MC_2B_{10} species; (iii) in contrast, reduction of 1,12-*closo*-C_2B_{10} carborane affords [7,10-*nido*-C_2B_{10}]$^{2-}$ and thus 4,1,10-MC_2B_{10} clusters upon metalation.[6a] Thermolysis of these kinetic metallacarborane isomers causes rearrangement to thermodynamically preferred ones; heating 4,1,6-MC_2B_{10} results, for some metals, in progressive conversion to 4,1,8- and then 4,1,12-MC_2B_{10} isomers,[12] and thermolysis of 4,1,10-MC_2B_{10} has been shown to produce the 4,1,12- isomer.[6a] A final known isomer is 4,1,2-MC_2B_{10}. This form is afforded either by direct insertion of a highly nucleophilic metal fragment into a 1,2-*closo*-C_2B_{10} cage[13] or by reduction and then metalation of a *C,C*-tethered 1,2-C_2B_{10} species.[8]

Focusing only on the metal coordination sphere we therefore now have access to four types of supraicosahedral MC_2B_{10} metallacarboranes. In three of these the metal fragment is bonded to C_2B_4 ligand faces with the cage C atoms either adjacent, **III** (the isomer 4,1,2-MC_2B_{10}); separated by a single B atom, **IV** (the isomer 4,1,6-MC_2B_{10}); or separated by two B atoms, **V** (the isomer 4,1,10-MC_2B_{10}) (see Chart 2). In the fourth type of MC_2B_{10} metallacarborane the metal is bound to a CB_5 ligand face, **VI** (the isomers 4,1,8- or 4,1,12-MC_2B_{10}).

Chart 2

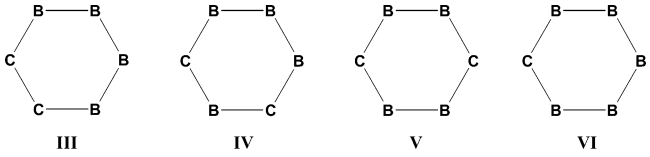

III **IV** **V** **VI**

Several years ago one of us was involved with studies into the conformational preferences and slipping distortions of $\{ML_2\}$ fragments (M = group 10 metal; L = 2e ligand, e.g., PR_3) with respect to five-atom carborane ligand faces (C_2B_3 faces with both adjacent and nonadjacent C atoms, and the CB_4 face) in icosahedral metallacarboranes.[14] In the present paper we describe, by a joint experimental and computational study, the ways in which $\{ML_2\}$ fragments now bond to the four different types of six-atom carborane faces (**III**−**VI** above) in supraicosahedral metallacarboranes, extending and complementing the earlier work.

Experimental Section

Synthesis: General. Experiments were performed under dry, oxygen-free N_2 using standard Schlenk techniques, with some subsequent manipulation in the open laboratory. Solvents were freshly distilled over CaH_2 (CH_2Cl_2) or Na wire (THF, 40−60 petroleum ether) or stored over 4 Å molecular sieves ($CDCl_3$, CD_2Cl_2) and were degassed (3 × freeze−pump−thaw cycles) before use. Preparative thin layer chromatography (TLC) employed 20 cm × 20 cm Kieselgel 60 F_{254} glass plates. For compounds **3** and **6** IR spectra were recorded from CH_2Cl_2 solutions using a Perkin-Elmer Spectrum RX FT spectrophotometer, and ^{1}H NMR spectra were recorded at 200.1 MHz (Bruker AC200 spectrometer) and ^{31}P and ^{11}B spectra at 162.0 and 128.4 MHz, respectively (Bruker DPX400 spectrometer) from $CDCl_3$ solutions at room temperature (Heriot-Watt University). For compound **8** IR spectra were recorded from CH_2Cl_2 solutions using a Bruker IFS25 FT spectrophotometer, and NMR spectra were recorded from CD_2Cl_2 solutions using a Bruker AMX360 spectrometer at 360.1, 115.5, and 90.6 MHz for ^{1}H, ^{11}B, and ^{13}C, respectively (Baylor University). Elemental analyses were determined by the appropriate departmental or commercial services. The starting materials 1,2-$(CH_2)_3$-1,2-*closo*-$C_2B_{10}H_{10}$,[15] [codRhCl]$_2$,[16] and $(PMe_2Ph)_2PtCl_2$[17] were prepared by literature methods or slight variations thereof. All other reagents and solvents were supplied commercially and used as received.

4,4-$(PMe_2Ph)_2$-4,1,6-*closo*-$PtC_2B_{10}H_{12}$. 1,2-*closo*-$C_2B_{10}H_{12}$ (0.045 g, 0.31 mmol) and freshly cut sodium (0.015 g, 0.68 mmol) were stirred in THF (∼20 mL) for 18 h. The resulting solution of $Na_2[C_2B_{10}H_{12}]$ was separated from excess sodium by cannula into a cooled (0 °C) suspension of $(PMe_2Ph)_2PtCl_2$ (0.15 g, 0.31 mmol) in THF (∼20 mL). The reactants were allowed to warm to room temperature and stirred for 18 h. Volatiles were removed in vacuo, leaving a yellow solid which was subsequently dissolved in CH_2Cl_2 (20 mL), filtered, and concentrated. Preparative TLC eluting with CH_2Cl_2/40−60 petroleum ether (1:1) afforded, as major product, a pale-yellow band (R_f = 0.15) subsequently shown to be 4,4-$(PMe_2Ph)_2$-4,1,6-*closo*-$PtC_2B_{10}H_{12}$, com-

(9) (a) Getman, T. D.; Knobler, C. B.; Hawthorne, M. F. *Inorg. Chem.* **1990**, *29*, 158. (b) McKee, M. L.; Bühl, M.; Schleyer, P. v. R. *Inorg. Chem.* **1993**, *32*, 1712. (c) Hermansson, K.; Wójcik, M.; Sjöberg, S. *Inorg. Chem.* **1999**, *38*, 6039.

(10) Representative examples: (a) Hewes, J. D.; Knobler, C. B.; Hawthorne, M. F. *J. Chem. Soc., Chem. Commun*. **1981**, 206. (b) Khattar, R.; Knobler, C. B.; Hawthorne, M. F. *J. Am. Chem. Soc.* **1990**, *112*, 4962. (c) Khattar, R.; Knobler, C. B.; Hawthorne, M. F. *Inorg. Chem.* **1990**, *29*, 2191. (d) Khattar, R.; Knobler, C. B.; Johnson, S. E.; Hawthorne, M. F. *Inorg. Chem.* **1991**, *30*, 1970. (e) Khattar, R.; Manning, M. J.; Knobler, C. B.; Johnson, S. E.; Hawthorne, M. F. Inorg. *Chem.* **1992**, *31*, 268. (f) Carr, N.; Mullica, D. F.; Sappenfield, E. L.; Stone, F. G. A.; Went, M. J. *Organometallics* **1993**, *12*, 4350. (g) Li, S.; Mullica, D. F.; Sappenfield, E. L.; Stone, F. G. A. *J. Organometal. Chem.* **1994**, *467*, 95. (h) Mullica, D. F.; Sappenfield, E. L.; Stone, F. G. A.; Woollam, S. F. *Can. J. Chem.* **1995**, *73*, 909. (i) Chui, K.; Yang, Q.; Mak, T. C. W.; Xie, Z. *Organometallics* **2000**, *19*, 1391. (j) Wilson, N. M. M.; Ellis, D.; Boyd, A. S. F.; Giles, B. T.; Macgregor, S. A.; Rosair, G. M.; Welch, A. J. *Chem. Commun*. **2002**, 464. (k) Burke, A.; Ellis, D.; Ferrer, D.; Ormsby, D. L.; Rosair, G. M.; Welch, A. J. *Dalton Trans.* **2005**, 1716.

(11) Dunks, G. B.; Wiersema, R. J.; Hawthorne, M. F. *J. Am. Chem. Soc.* **1973**, *95*, 3174.

(12) (a) Dustin, D. F.; Dunks, G. B.; Hawthorne, M. F. *J. Am. Chem. Soc.* **1973**, *95*, 1109. (b) Burke, A.; McIntosh, R.; Ellis, D.; Rosair, G. M.; Welch, A. J. *Collect. Czech. Chem. Commun.* **2002**, *67*, 991.

(13) Barker, G. K.; Garcia, M. P.; Green, M.; Stone, F. G. A.; Welch, A. J. *J. Chem. Soc., Chem. Commun*. **1983**, 137.

(14) (a) Mingos, D. M. P.; Forsyth, M. I.; Welch, A. J. *J. Chem Soc., Chem. Commun*. **1977**, 605. (b) Mingos, D. M. P.; Forsyth, M. I.; Welch, A. J. *J. Chem. Soc., Dalton Trans.* **1978**, 1363.

(15) Paxon, T. E.; Kaloustian, M. K.; Tom, G. M.; Wiersema, R. J.; Hawthorne, M. F. *J. Am. Chem. Soc.* **1972**, *94*, 4882.

(16) Chatt, J.; Venanzi, L. M. *J. Chem. Soc.* **1957**, 4735.

(17) Jenkins, J. M.; Shaw, B. L. *J. Chem. Soc. (A)* **1966**, 770.

pound **3**, (0.38 g, 20%). $C_{18}H_{34}B_{10}P_2Pt$ requires C 35.1, H 5.58. Found: C 35.2, H 5.60. IR, ν_{max} at 2500 cm^{-1} (B−H). $^{11}B\{^1H\}$ NMR: δ −0.98 (2B), −2.60 (1B), −4.54 (3B), −9.46 (1B), −13.85 (2B), and −15.00 $\langle\delta(^{11}B)\rangle = -11.62$. ^1H NMR, δ 7.45−7.25 (m, 10H, C_6H_5), 3.95 (br s, 2H, $C_{cage}H$), and 1.7−1.3 (br m, 12H, $P(CH_3)_2$). $^{31}P\{^1H\}$ NMR: δ −17.61 (s, J_{PtP} 3894 Hz) and −20.82 (s, J_{PtP} 2800 Hz).

4,4-(PMe$_2$Ph)$_2$-4,1,10-*closo*-PtC$_2$B$_{10}$H$_{12}$. 1,12-*closo*-$C_2B_{10}H_{12}$ (0.10 g, 0.69 mmol) was cooled to −80 °C. Ammonia (~20 mL) and freshly cut sodium (0.13 g, 5.6 mmol) were added, and the resulting dark-blue solution was stirred for 2 h. Following removal of the ammonia in vacuo the residue was extracted into THF (20 mL) and transferred, by cannula, to a frozen solution of $(PMe_2Ph)_2PtCl_2$ (0.37 g, 0.69 mmol) in THF (20 mL). The reaction mix was allowed to warm to room temperature and stirred for 30 min (**warning − prolonged stirring leads to significant decomposition!**). Volatiles were removed in vacuo, and the yellow residue was extracted into CH_2Cl_2 (20 mL), filtered, and then purified by preparative TLC eluting with CH_2Cl_2/40−60 petroleum ether (7:3) to afford, as a narrow yellow band (R_f = 0.29), the compound 4,4-(PMe$_2$Ph)$_2$-4,1,10-*closo*-$PtC_2B_{10}H_{12}$, compound **6**, (0.02 g, 10%). IR, ν_{max} at 2529 cm^{-1} (B−H). $^{11}B\{^1H\}$ NMR: δ 15.91 (2B), 11.04 (1B), 0.17 (1B), −8.38 (2B), −16.30 (2B) and −22.83 (2B), $\langle\delta(^{11}B)\rangle = 0.36$. ^1H NMR: δ 7.6−7.1 (m, 10H, C_6H_5), 4.3 (br s, 1H, $C_{cage}H$), 2.7 (br s, 1H, $C_{cage}H$) and 1.9−1.2 (br m, 12H, $P(CH_3)_2$). $^{31}P\{^1H\}$ NMR: δ −13.16 (s, J_{PtP} 3013 Hz).

[N(PPh$_3$)$_2$][4,4-cod-4,1,10-*closo*-RhC$_2$B$_{10}$H$_{12}$]. Similarly, from 1,12-*closo*-$C_2B_{10}H_{10}$ (0.20 g, 1.39 mmol) and $[codRhCl]_2$ (0.34 g, 0.69 mmol), followed by metathesis with $[N(PPh_3)_2]Cl$ (0.80 g, 1.39 mmol) was isolated yellow $[N(PPh_3)_2][4,4\text{-cod-}4,1,10\text{-}closo\text{-}RhC_2B_{10}H_{12}]$, salt **8**, (0.50 g, 40%) as the major mobile product following column chromatography (eluting with CH_2Cl_2/40−60 petroleum ether, 7:3). $C_{46}H_{54}B_{10}NP_2Rh$ requires C 61.8, H 6.1, N 1.6. Found: C 62.0, H 6.2, N 1.7. IR: ν_{max} at 2531 cm^{-1} (B−H). $^{11}B\{^1H\}$ NMR (CD_2Cl_2) δ −4.5 (2B), −6.0 (2B), −12.3 (1B), −13.5 (1B), −16.2 (2B) and −17.2 (2B), $\langle\delta(^{11}B)\rangle = -11.4$. ^1H NMR (CD_2Cl_2): δ 7.8−7.5 (m, 30H, C_6H_5), 5.06 (vbr, 1H, $C_{cage}H$), 4.35 (br, 4H, =C*H*), 2.22 (br, 8H, CH_2), and 2.05 (vbr, 1H, $C_{cage}H$). $^{13}C\{^1H\}$ NMR (CD_2Cl_2): 133.8−126.5 (C_6H_5), 79.0 (br, C_{cage}), 77.1 [d, J(RhC) 10 Hz, =*C*H], 42.4 (br, C_{cage}) and 32.2 (CH_2).

Crystallography. Intensity data were collected on single crystals of **3**, **6**, and **8**·1/2CH_2Cl_2 on a Bruker X8 APEX2 diffractometer,[18] with crystals mounted in inert oil on a glass fiber and cooled to 100 K (**3** and **6**, Heriot-Watt University) or 110 K (**8**, Baylor University) by an Oxford Cryosystems Cryostream. The structures were solved by direct methods and refined by full-matrix least-squares.[19] All non-H atoms were refined with anisotropic displacement parameters. In compound **6** the cage is disordered about a crystallographic C_2 axis, and the disorder was modeled by two intersecting half-occupancy pentagonal pyramids for the lower cage belt (B5B9B12B13B8B11), co-incident at the (crystallographically equivalent) B8 and B9 positions. In spite of this disorder C1 (≡ C10) was unambiguously identified as a carbon atom. For **3** and **8** cage-bound H atoms were located in difference Fourier maps and freely refined, but with thermal parameters set to 1.2 × U_{eq} of the attached B or C atom. In the case of **6**, some cage B*H* atoms were located and positionally refined, but restrained to B−H 1.10(2) Å, while others were set in calculated positions; the position of the single CH was also calculated, with C−H 1.10 Å; again, thermal parameters for all cage H atoms were set to 1.2 × U_{eq} of the attached B or C atom. Note that, although B11 is disordered over two positions, its attached H atom sits on the crystallographic C_2 axis. In **3** and **6**, methyl H atoms (C−H 0.98 Å) and phenyl H atoms (C−H 0.95 Å) were placed in calculated but riding positions, with U_H set to 1.5 or 1.2 × U_{eqC}, respectively. For **8**, non-cage H atoms were set in calculated, riding positions, with C−H 0.95 (phenyl), 0.99 (CH_2) or 1.00 (cod-CH) Å, and U_H set to 1.2 × U_{eqC}. The CH_2Cl_2 of solvation of **8** is disordered about an inversion center and was refined with C−Cl restrained to 1.76(2) Å. Table 1 contains further experimental details.

Table 1. Crystallographic Data

	3	**6**	**8**·1/2CH_2Cl_2
formula	$C_{18}H_{34}B_{10}P_2Pt$	$C_{18}H_{34}B_{10}P_2Pt$	$C_{46.5}H_{55}B_{10}ClNP_2Rh$
M_r	615.58	615.58	936.22
system	monoclinic	monoclinic	triclinic
space group	$P2_1/c$	$C2/c$	$\bar{P}$
a/Å	13.6694(9)	20.335(3)	10.056(5)
b/Å	10.5522(7)	10.4382(14)	14.692(7)
c/Å	17.3895(12)	13.5990(19)	17.296(13)
α/deg	90	90	113.67(4)
β/deg	100.028(3)	122.496(3)	100.35(4)
γ/deg	90	90	98.26(3)
V/Å^3	2470.0(3)	2434.6(6)	2235(2)
Z	4	4	2
D_c/Mg m^{-3}	1.655	1.679	1.391
μ/mm^{-1}	5.816	5.901	0.550
F(000)	1200	1200	966
θ_{max}	33.22	36.29	27.64
data measured	34349	63206	45526
unique data, n	9430	5859	10159
R_{int}	0.0229	0.0464	0.0664
max, min. tfs	0.498, 0.315	0.702, 0.566	0.921, 0.803
R1[a]	0.0182	0.0378	0.0601
wR2[a]	0.0397	0.0523	0.1199
S[a]	1.184	0.923	0.998
variables, p	320	169	596
$\Delta\rho_{max}$, $\Delta\rho_{min}$/e Å^{-3}	2.087, −1.294	3.261, −1.891	1.801, −1.745

[a] $R1 = \sum(|F_o| - |F_c|)/\sum|F_o|$, $wR2 = [\sum[w(F_o^2 - F_c^2)^2]/\sum w(F_o^2)^2]^{1/2}$, $S = [\sum[w(F_o^2 - F_c^2)^2/(n-p)]^{1/2}$, where n is the number of data and p the number of parameters. R1 and wR2 quoted for *all* data.

Calculations. All geometries were optimized at the B3LYP[20] level with the basis set for all atoms of double-ζ quality. For carbon, hydrogen, and boron Pople's 6-31G(d,p) basis set was used, while for platinum and phosphorus the Stuttgart relativistic ECP[21] was employed with an additional d-polarization function on phosphorus.[22] Frequency calculations were performed to determine the nature of the optimized geometries. The Gaussian 03 program[23] was used for all calculations. Optimized geometries are displayed via Mercury.[24]

Results and Discussion

This paper is concerned with the conformations of nine 13-vertex metallacarboranes, compounds **1**−**9**. Six of these compounds (**1**, **2**, **4**, **5**, **7**, and **9**) have already been described in the literature (although their conformations were not discussed), and three (**3**, **6** and **8**) are new. The compounds are summarized in Table 2 and sketched in Chart 3.

1. Synthesis and Characterization. 4,1,2-MC$_2$B$_{10}$ Compounds. The synthesis, spectroscopic characterization, and structural studies of the platina- and nickelacarboranes 1,2-$(CH_2)_3$-4,4-$(PMe_2Ph)_2$-4,1,2-*closo*-$PtC_2B_{10}H_{10}$, **1**, and 1,2-$(CH_2)_3$-4,4-dppe-4,1,2-*closo*-$NiC_2B_{10}H_{10}$, **2**, (dppe = $Ph_2PCH_2CH_2PPh_2$)

(18) *Bruker AXS APEX2*, version 1.0-8; Bruker AXS Inc.: Madison, WI, U.S.A., 2003.
(19) Sheldrick, G. M. *SHELXTL*, versions 5.1 and 6.12; Bruker AXS Inc.: Madison, WI, U.S.A., 1999 and 2001, respectively.
(20) (a) Becke, A. D. *J. Chem. Phys.* **1993**, *98*, 1372. (b) Becke, A. D. *J. Chem. Phys.* **1993**, *98*, 5648. (c) Lee, C.; Yang, W.; Parr, R. G. *Phys. Rev. B* **1988**, *37*, 785. (d) Becke, A. D. *Phys. Rev. A* **1988**, *38*, 3098.
(21) (a) Bergner, A.; Dolg, M.; Kuechle, H.; Stoll, H.; Preuss, H. *Mol. Phys.* **1993**, *80*, 1431. (b) Kaupp, M.; Schleyer, P. v. R.; Stoll, H.; Preuss, H. *J. Chem. Phys.* **1991**, *94*, 1360. (c) Dolg, M.; Stoll, H.; Preuss, H.; Pitzer, R. M. *J. Phys. Chem.* **1993**, *97*, 5852.
(22) Höllwarth, A.; Böhme, M.; Dapprich, S.; Ehlers, A. W.; Gobbi, A.; Jonas, V.; Köhler, K. F.; Stegmann, R.; Veldkamp, A.; Frenking, G. *Chem. Phys. Lett.* **1993**, *208*, 237.
(23) Frisch, M. J., *et al*. *Gaussian 03, revision C.02*; Gaussian Inc., Wallingford, CT, U.S.A., 2004.
(24) *Mercury*, version 1.4.1; Cambridge Crystallographic Data Center: Cambridge, UK, 2006.

Table 2. Summary of Compounds Described

	4,1,2-[*M*]C_2B_{10} (ligand type **III**)	4,1,6-[*M*]C_2B_{10} (ligand type **IV**)	4,1,10-[*M*]C_2B_{10} (ligand type **V**)	4,1,12-[*M*]C_2B_{10} (ligand type **VI**)
[*M*] = P_2Pt[a]	**1**	**3**	**6**	
[*M*] = dppeNi	**2**	**4**	**7**	**9**
[*M*]$^-$ = codRh		**5**	**8**	

[a] P = PMe_2Ph

Chart 3

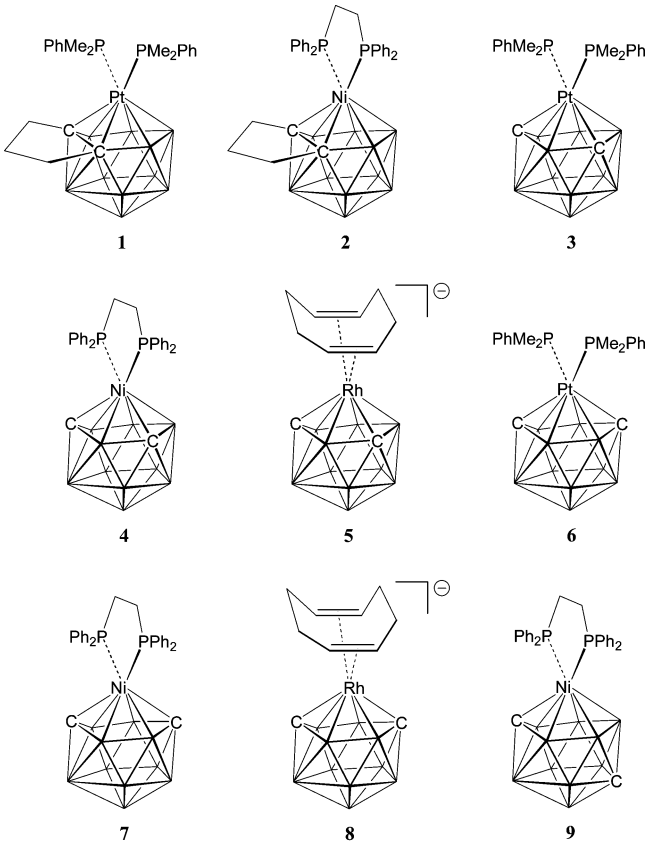

Unlabeled cage vertices are BH
Except for **1** and **2** cage C vertices are CH

were described recently.[8] The cages in both these metallacarboranes are docosahedral with formal connectivities between C2 and B5, although that for **1** is relatively long, 2.055(12) Å, consistent with a distortion toward a henicosahedral cage.

Figure 1 shows views of the central $ML_2C_2B_4$ portions of **1** and **2**, illustrating the conformations of the {ML_2} fragments relative to the C_2B_4 ligand face. A convenient (arbitrary) quantitative measure of these conformations is θ, the dihedral angle between ML_2 and *M*C1B10B11 (compounds **1**−**5**, **9**) or *M*C1C10B11 (compounds **6**−**8**) planes, where $0 < \theta < 90°$ represents, in projection, one ligand *L* lying in the B3 quadrant, and $90 < \theta < 180°$ represents *L* in the B7 quadrant. For compounds **1** and **2** θ is 61.1° and 64.6°, respectively.

All attempts to prepare [1,2-$(CH_2)_3$-4,4-cod-4,1,2-*closo*-$RhC_2B_{10}H_{10}]^-$, the rhodacarborane anion analogue of **1** and **2**, were unsuccessful.

4,1,6-*M*C_2B_{10} Compounds. We have prepared the platinum complex 4,4-$(PMe_2Ph)_2$-4,1,6-*closo*-$PtC_2B_{10}H_{12}$, **3**, to complement its previously described analogues, namely the nickelacarborane 4,4-dppe-4,1,6-*closo*-$NiC_2B_{10}H_{12}$, **4**,[25] and the rhodacarborane salt $[N(PPh_3)_2]$[4,4-cod-4,1,6-*closo*-$RhC_2B_{10}H_{12}$], **5**.[26] Sodium reduction of 1,2-*closo*-1,2-$C_2B_{10}H_{12}$ followed by treatment with $(PMe_2Ph)_2PtCl_2$ and workup involving TLC affords the yellow compound **3** in reasonable yield. The $^{11}B\{^1H\}$ NMR spectrum of **3** reveals six resonances between δ 0 and −15, with relative integrals 2:1:3[2+1 co-incidence]:1:2:1 (from high frequency to low frequency) and with a weighted average ^{11}B chemical shift, $\langle\delta(^{11}B)\rangle$, of −11.6. In the ^1H NMR spectrum is a single resonance for cage C*H* atoms, δ 3.95, whereas the $^{31}P\{^1H\}$ NMR spectrum reveals two singlets (with attendant ^{195}Pt satellites) at δ −17.6 and −20.8. All these data are consistent with a (time-averaged) structure in solution of C_s symmetry, with the PtP_2 plane lying on the molecular mirror plane.

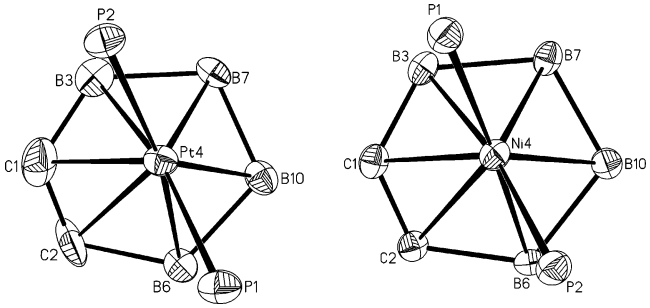

Figure 1. Experimental conformations of the {MP_2} fragments in (left) **1** (θ = 61.1°) and (right) **2** (θ = 64.6°).

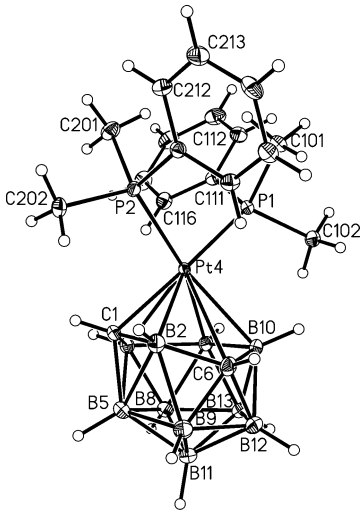

Figure 2. Perspective view of compound **3**. Thermal ellipsoids are drawn at the 50% probability level, except for H atoms which have an artificial radius for clarity.

Compound **3** was further characterized by a crystallographic study. Figure 2 contains a perspective view of the compound, and Table 3 lists selected molecular parameters. The cage of **3**, like that of **4** and **5**, is a docosahedron, but is considerably distorted by, in particular, a very long Pt4···C6 distance, 2.813(13) Å. Note that the Pt4−C6 vector, in projection (see Figure 3, left) lies effectively perpendicular to the PtP_2 plane. B−B distances within **3** follow the trends already established[10k,25] for 4,1,6-*M*C_2B_{10} polyhedra, with connectivities involving the degree-six B atom B5 being relatively long, particularly so if

(25) Laguna, M. A.; Ellis, D.; Rosair, G. M.; Welch, A. J. *Inorg. Chim. Acta* **2003**, *347*, 161.
(26) Hodson, B. E.; McGrath, T. D.; Stone, F. G. A. *Organometallics* **2005**, *24*, 1638.

Table 3. Selected Molecular Parameters (Å, deg) in 4,4-$(PMe_2Ph)_2$-4,1,6-*closo*-$PtC_2B_{10}H_{12}$, **3**

C1−B2	1.555(2)	Pt4···C6	2.8131(13)	B8−B11	1.766(2)
C1−B3	1.573(2)	Pt4−B7	2.2631(14)	B8−B13	1.758(2)
C1−Pt4	2.1652(12)	Pt4−B10	2.3692(14)	B9−B11	1.730(3)
C1−B5	1.742(2)	B5−B8	1.867(2)	B9−B12	1.750(2)
B2−Pt4	2.4438(15)	B5−B9	1.957(3)	B10−B12	1.827(2)
B2−B5	2.259(3)	B5−B11	1.804(2)	B10−B13	1.816(2)
B2−C6	1.623(2)	C6−B9	1.662(2)	B11−B12	1.785(2)
B2−B9	1.932(2)	C6−B10	1.693(2)	B11−B13	1.802(2)
B3−Pt4	2.3961(14)	C6−B12	1.647(2)	B12−B13	1.768(3)
B3−B5	1.884(2)	B7−B8	1.783(2)	Pt4−P1	2.2710(3)
B3−B7	1.856(2)	B7−B10	1.862(2)	Pt4−P2	2.3129(4)
B3−B8	1.752(2)	B7−B13	1.764(2)	P1−Pt4−P2	92.363(14)

the other B atom is also connected to the degree-six Pt atom and one or more cage C atoms. Thus, B2−B5, 2.259(3) Å, is the longest, followed by B9−B5, 1.957(3) Å, B3−B5, 1.884(2) Å, and B8−B5, 1.867(2) Å. In **3** the conformation of the PtP_2 plane is defined by $\theta = 148.7°$.

The C_s symmetry of the cage of **3** implied by the NMR data can be readily understood in terms of the double diamond−square−diamond fluxional process first suggested by Hawthorne for the CpCo system[12a] and recently confirmed computationally by us for the Sn[10j] and (η-C_6H_6)Ru[10k] systems. This process effectively generates a mirror plane through atoms Pt4, B2, B11, and B7 (the integral-1 B atoms), which relates pairwise B3 and B10, B5 and B9, and B8 and B12 (the integral-2 B atoms) and renders equivalent the two cage C atoms. To maintain the inequivalence of the P atoms all that is required is a synchronous libration of the PtP_2 unit about the Pt4B2B7 plane (see Figure 3). Full rotation of the {PtP_2} fragment, which would render the P atoms equivalent, presumably occurs at higher temperatures, but this was not explored as attempts to isomerize **3** by thermolysis (see later) led only to decomposition.

Compound **4** crystallizes (as its 1:1 CH_2Cl_2 solvate) in two crystalline modifications, **4**α and **4**β, but the cages of the two forms are practically superimposable. The angle θ, defined as above, is 134.6° for **4**α and 136.7° for **4**β. Figure 3 (left and center) shows views of the $MP_2C_2B_4$ cores of **3** and **4**α, comparing the orientation of the MP_2 planes relative to the carborane ligand faces. To describe the conformation of the {codRh} fragment in the anion of **5** we define X1 and X2 as the midpoints of the cod C═C bonds. Figure 3 (right) is a view of the $RhX_2C_2B_4$ central part of the anion of **5**, and θ, the dihedral angle between the RhX_2 and RhC1B10B11 planes, is 115.1°.

4,1,10-*M*C_2B_{10} Compounds. The nickelacarborane 4,4-(dppe)-4,1,10-*closo*-$NiC_2B_{10}H_{12}$, **7**, afforded by nickelation of reduced 1,12-*closo*-$C_2B_{10}H_{12}$, has been reported in a recent

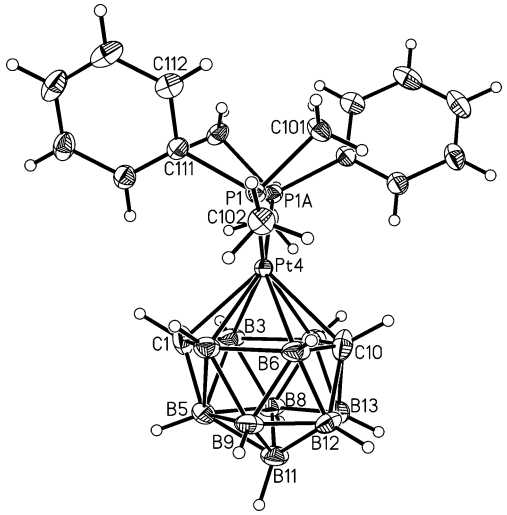

Figure 4. Perspective view of compound **6** showing, for clarity, only one of the disordered pentagonal pyramids used to model the lower part of the molecule. Thermal ellipsoids as for Figure 2. Note that the polyhedral numbering in this Figure is conventional and not necessarily that in the corresponding CIF.

communication.[6a] Similar treatment of the [7,10-*nido*-$C_2B_{10}H_{12}]^{2-}$ anion with $(PMe_2Ph)_2PtCl_2$ or with $[codRhCl]_2$ (the latter followed by cation metathesis) yields the yellow platina- and rhodacarborane species 4,4-$(PMe_2Ph)_2$-4,1,10-*closo*-$PtC_2B_{10}H_{12}$, **6**, and [$N(PPh_3)_2$][4,4-cod-4,1,10-*closo*-$RhC_2B_{10}H_{12}$], **8**, following chromatographic workup. The isolated yield of **6** is relatively poor, but the compound is comparatively unstable. The yield of **8** is reasonable, and certainly **8** is the major reaction product.

NMR spectra of **6** are fully consistent with a C_s symmetric compound. In the $^{11}B\{^1H\}$ spectrum are six resonances, 2:1:1:2:2:2 (high to low frequency), between δ +16 and −23, with $\langle\delta(^{11}B)\rangle = 0.4$, and the $^{31}P\{^1H\}$ spectrum yields a singlet (with attendant ^{195}Pt satellites) at δ −13.6. There are two cage C*H* resonances in the ^1H spectrum, at δ 4.3 and 2.7, implying that these lie on the mirror plane and not across it. A crystallographic study of **6** is fully consistent with these conclusions, but unfortunately suffers from partial disorder of the lower {B_6H_6} fragment, which has been modeled as two interpenetrating pentagonal pyramids (see Experimental Section). Figure 4 is a perspective view of one molecule of **6** in which only one of these lower pentagonal pyramids is shown. Table 4 lists key molecular parameters. Crystallographically, the disordered model has precise C_2 symmetry, but (both) the disordered components also have effective C_s symmetry, at least as far as the $P_2PtC_2B_{10}$ fragments are concerned. Although the disorder is also manifest in the upper C_2B_4 portion of the carborane ligand

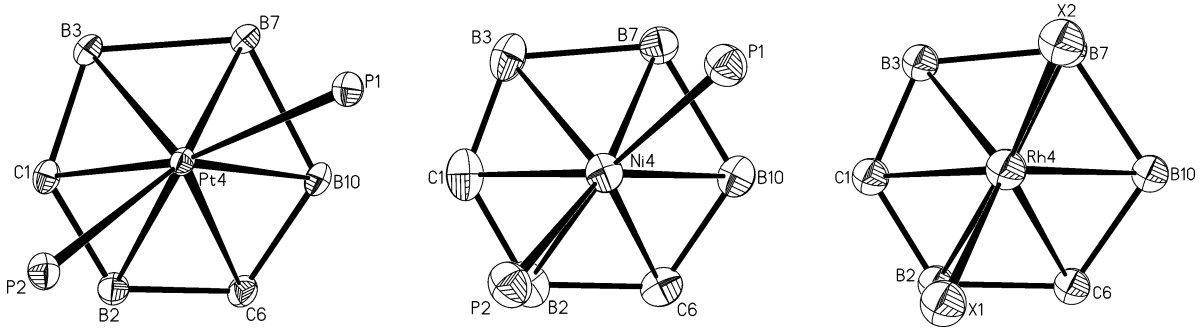

Figure 3. Experimental conformations of the {ML_2} fragments in **3** (left; $\theta = 148.7°$), **4**α (center; $\theta = 134.6°$) and **5** (right; $\theta = 115.1°$).

Table 4. Selected Molecular Parameters (Å, deg) in 4,4-$(PMe_2Ph)_2$-4,1,10-*closo*-$PtC_2B_{10}H_{12}$, **6**

C1−B2	1.599(3)	B3−B5	2.117(6)	B8−B13	1.714(6)
C1−B3	1.611(4)	B3−B8	1.781(3)	B9−B12	1.666(6)
C1−Pt4	2.357(2)	B5−B8	1.983(7)	C10−B12	1.815(5)
C1−B5	1.635(6)	B5−B9	1.881(6)	C10−B13	1.747(5)
B2−Pt4	2.337(2)	B5−B11	1.777(7)	B11−B12	1.762(7)
B2−B5	2.055(5)	B6−B12	1.694(5)	B11−B13	1.762(9)
B2−B6	1.853(4)	B7−B13	1.750(5)	B12−B13	1.751(7)
B2−B9	1.801(3)	B8−B11	1.783(7)	Pt4−P1	2.2937(5)
				P1−Pt4−P1A	91.87(2)

in that the formally degree-four and degree-five atoms C1 and C10 are crystallographically equivalent, the disorder does not influence the broad conclusion regarding the conformation of the PtP_2 unit with respect to the C_2B_4 ligand face (Figure 5 left). θ for **6** is 87.7°. Detailed analysis of the structure of **6** is not warranted because of the crystallographic disorder, save to note very long B2−B5 and B3−B5 and long B8−B5 and B9−B5 distances. These typical aspects of 4,1,10-MC_2B_{10} compounds are more fully discussed below.

The $^{11}B\{^1H\}$ NMR spectrum of **7** was relatively uninformative (only three broad peaks with relative integrals 4:1:5), but importantly, there is only a single resonance in the $^{31}P\{^1H\}$ NMR spectrum.[6a] The crystallographically determined molecular structure reveals a docosahedral cage with the phosphine ligands symmetrically disposed about an effective mirror plane passing through C1, Ni4, C10, and B11. This is clearly visible in Figure 5 center, a view of the nickel co-ordination sphere. As anticipated for such an orthogonal arrangement, the parameter θ for compound **7** is 89.4°.

The $^{11}B\{^1H\}$ NMR spectrum of **8** differs from that of **6** in that the relative integrals are slightly altered (2:2:1:1:2:2) and the whole spectrum is compressed and shifted to low frequency (δ −4 to −18, $\langle\delta(^{11}B)\rangle = -11.4$), the latter anticipated for an anionic metallacarborane. In the ^1H spectrum the two cage C*H* resonances are again well separated, δ 5.1 and 2.1, and the different nature of the two cage {CH} units is further reinforced by very different chemical shifts in the $^{13}C\{^1H\}$ spectrum, δ 79.0 and 42.4.

The docosahedral nature of the cage and the 4,1,10-RhC_2 heteroatom pattern are confirmed by a crystallographic study (Figure 6 and Table 5). This confirms that the anion has near C_s symmetry about the plane defined by Rh4, C1, C10, and B11. In common with recent structural studies on related (ordered) 4,1,10-[*M*]C_2B_{10} species ([*M*] = CoCp, Ru(*p*-cymene), Nidppe),[5a] the B2−B5 and B3−B5 connectivities in **8** are very

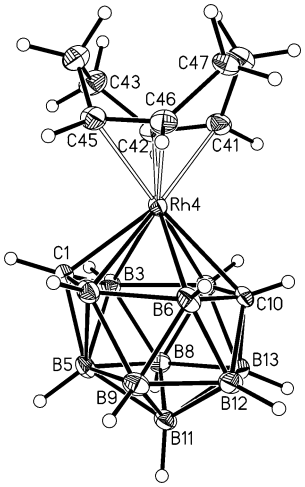

Figure 6. Perspective view of the anion of **8**, with thermal ellipsoids as for Figure 2.

Table 5. Selected Interatomic Distances (Å) in the $[4,4\text{-cod-}4,1,10\text{-}closo\text{-}RhC_2B_{10}H_{12}]^-$ Anion of **8**

C1−B2	1.527(5)	Rh4−B7	2.235(4)	B9−B11	1.729(5)
C1−B3	1.534(5)	Rh4−C10	2.302(3)	B9−B12	1.718(5)
C1−Rh4	2.177(3)	B5−B8	1.885(5)	C10−B12	1.706(5)
C1−B5	1.761(5)	B5−B9	1.915(5)	C10−B13	1.695(5)
B2−Rh4	2.266(4)	B5−B11	1.782(5)	B11−B12	1.774(5)
B2−B5	2.072(5)	B6−B9	1.763(5)	B11−B13	1.778(5)
B2−B6	1.813(5)	B6−C10	1.669(5)	B12−B13	1.743(5)
B2−B9	1.834(5)	B6−B12	1.756(5)	Rh4−C41	2.169(3)
B3−Rh4	2.350(4)	B7−B8	1.781(5)	Rh4−C42	2.167(3)
B3−B5	1.967(5)	B7−C10	1.674(4)	Rh4−C45	2.151(3)
B3−B7	1.858(5)	B7−B13	1.770(5)	Rh4−C46	2.158(3)
B3−B8	1.786(5)	B8−B11	1.756(5)	C41−C42	1.404(4)
Rh4−B6	2.284(4)	B8−B13	1.729(5)	C45−C46	1.406(4)

long, 2.072(5) and 1.967(5) Å, respectively, and the B8−B5 and B9−B5 distances long, 1.885(5) and 1.915(5) Å, respectively. Defining X1 as the midpoint of the C41═C42 bond and X2 as the midpoint of the C45═C46 bond, we note that the RhX_2 plane is slightly off perpendicular to the RhC1C10B11 plane, with $\theta = 104.2°$ (Figure 5 right). Pairwise across the effective mirror plane the B atom which is more closely trans to the alkene ligand is the more strongly bound to Rh, i.e., Rh4−B2 < Rh4−B3 and Rh4−B7 < Rh4−B6. The shortest Rh−B connectivity is to B7, and is accompanied by a small but clear trans influence in the Rh−C_{ene} bonding, with Rh−C45,46 measurably shorter than Rh−C41,42.

The $[N(PPh_3)_2]^+$ cation in **8** is ordered, with N−P distances of 1.563(3) and 1.575(3) Å, and P−N−P = 145.05(18)°. Salt

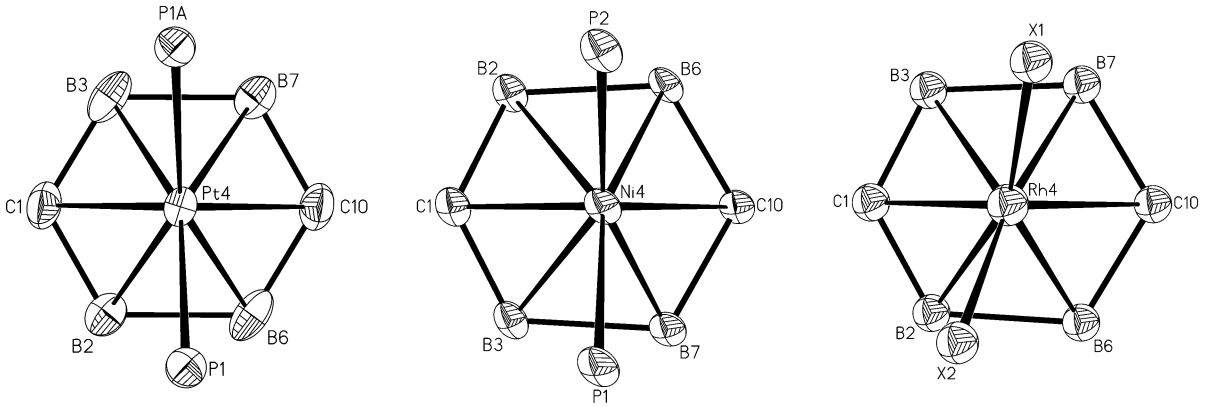

Figure 5. Experimental conformations of the $\{ML_2\}$ fragments in **6** (left; $\theta = 87.7°$), **7** (center; $\theta = 89.4°$) and **8** (right; $\theta = 104.2°$).

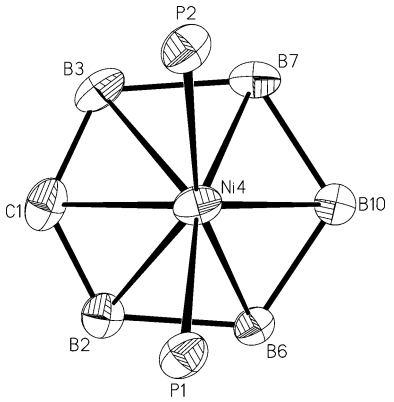

Figure 7. Experimental conformation of the $\{NiP_2\}$ fragment in **9**. θ = 90.0°.

8 cocrystallises with $^1/_2CH_2Cl_2$, disordered about a crystallographic inversion center.

4,1,12-*M*C_2B_{10} Compounds. The nickelacarborane 4,4-(dppe)-4,1,12-*closo*-$NiC_2B_{10}H_{12}$, **9**, is produced when the corresponding 4,1,10-isomer, compound **7**, is heated in refluxing toluene.[6a] Compound **9** has been characterized crystallographically.[6a] Although the structural determination suffers from partial disorder in one-half of the dppe ligand, it is nevertheless possible to define the conformation of the (major) NiP_2 plane relative to the plane through NiC1B10B11 as θ = 90.0° (Figure 7).

2. Conformations. The crystallographic studies described above reveal what appears to be a clear preference for the conformations of $\{ML_2\}$ fragments bonded to each of the four kinds of six-atom ligand faces in 13-vertex 4,1,*x*-*M*C_2B_{10} metallacarboranes. For ligand type **III** (4,1,2-*M*C_2B_{10}) θ is 61.1° (compound **1**) and 64.6° (**2**). For ligand **IV** (4,1,6-*M*C_2B_{10}) we observe θ = 148.7° (**3**), 134.6°, 136.7° (**4**), and 115.1° (**5**). Ligand type **V** (4,1,10-*M*C_2B_{10}) favors effectively perpendicular arrangements, with θ = 87.7° (**6**), 89.4° (**7**), and 104.2° (**8**), and this situation is maintained in the one example of ligand type **VI** (4,1,12-*M*C_2B_{10}), with θ = 90.0° in compound **9**. In this section we explore these conformations computationally.

In earlier studies of the conformations of $\{ML_2\}$ fragments in icosahedral metallacarboranes we described the conformations as parallel (||) or perpendicular (⊥) with respect to the mirror plane through the cage. When there are two adjacent cage C atoms in the ligating face, a ⊥ conformation is observed (**VII**, Chart 4).[14b] However, when the cage C atoms are nonadjacent, the alternative || conformation is seen (**VIII**).[27] Finally, in the case of a single C atom in the ligating face, the conformation returns to ⊥ (**IX**).[28]

In all cases we rationalized these observations by the results of MO calculations (at the extended Hückel level) which revealed[14] that:

(1) in carborane ligands the frontier molecular orbitals are localized primarily on the B atoms in the open face;

(2) partitioning the electrons as d^{10}-ML_2 (and consequently neutral *nido*-C_2B_9 or monoanionic *nido*-CB_{10} ligands), the metal fragment LUMO is an $s-p_z$ hybrid (**X**, Chart 5) and the HOMO an in-plane d−p hybrid (**XI**), both reinforced away from the P atoms. Clearly the metal LUMO has no conformational preference. The HOMO and HOMO−1 (**XII**), which is pure metal d character, have orthogonal conformational preferences; however, because of its hybridization, the HOMO has a greater interaction with the cage, and the overall conformation is set by the metal HOMO/cage LUMO interaction. For **VII** and **IX** as drawn above, the cage LUMO has a left−right nodal plane, and for **VIII** a top−bottom nodal plane, leading to ⊥ conformations in the cases of **VII** and **IX** and || in the case of **VIII**;

(3) the magnitude and direction of the slip distortion of the $\{ML_2\}$ fragment with respect to the cage is that which maximizes both sets of frontier orbital interactions.

Chart 4

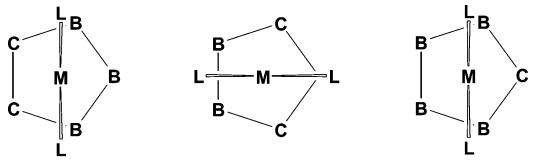

Chart 5

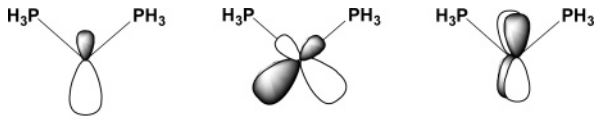

These early calculations were useful in that they rationalized the observed conformations in terms of simple symmetry-based arguments, appropriate since in the icosahedron all vertices are of degree-five. This, however, is not the case in the 13-vertex docosahedron and henicosahedron. Nevertheless, to allow optimal comparison with the icosahedral system we wanted to explore the conformations of ML_2 fragments with respect to six-atom carborane rings in which the B and C atoms were equally connected, and thus initial calculations focused on the 18-electron heteroarene complexes, $[(PH_3)_2PtC_2B_4H_6]^{2-}$ and $[(PH_3)_2PtCB_5H_6]^{3-}$. We attempted to optimize both || and ⊥ structures for all three isomers of the C_2B_4 species and for the CB_5 species, using DFT.

When the two C atoms are adjacent, i.e., the analogue of the C_2B_{10} ligand type **III**, and structures were minimized in C_s symmetry, the ⊥ form (Figure 8, left) was found to be a minimum. The || isomer (Figure 8, right) lies 4.4 kcal mol^{-1} above the ⊥ form, but the former is not a local minimum, having two imaginary frequencies which correspond to PH_3 rotation. If the symmetry constraint is relaxed, however, a further minimum with one C atom eclipsed by a PH_3 group (Figure 8, center) is located just +0.68 kcal mol^{-1} above the ⊥ structure. Note that the minimum (⊥) conformation corresponds to a form with θ = 60° and recall that in compounds **1** and **2** real examples of metallacarboranes incorporating the type **III** C_2B_{10} ligand measured θ values were 61.1° and 64.6°.

In Figure 9 (left) is shown the minimum energy structure, optimized in C_s symmetry, for the $[(PH_3)_2Pt(C_2B_4\text{-}1,3)]^{2-}$ species, the analogue of the platinacarborane **3** containing the C_2B_{10} carborane type **IV**. This || form is 19.1 kcal mol^{-1} more stable than the alternative ⊥ form (Figure 9, right) which corresponds to a transition state for $\{Pt(PH_3)_2\}$ rotation. The ||

(27) (a) Green, M.; Spencer, J. L.; Stone, F. G. A.; Welch, A. J. *J. Chem. Soc., Chem. Commun.* **1974**, 571. (b) Green, M.; Spencer, J. L.; Stone, F. G. A.; Welch, A. J. *J. Chem. Soc., Dalton Trans.* **1975**, 179. (c) Welch, A. J. *J. Chem. Soc., Dalton Trans.* **1975**, 1473.
(28) Carroll, W. E.; Green, M.; Stone, F. G. A.; Welch, A. J. *J. Chem. Soc., Dalton Trans.* **1975**, 2263.

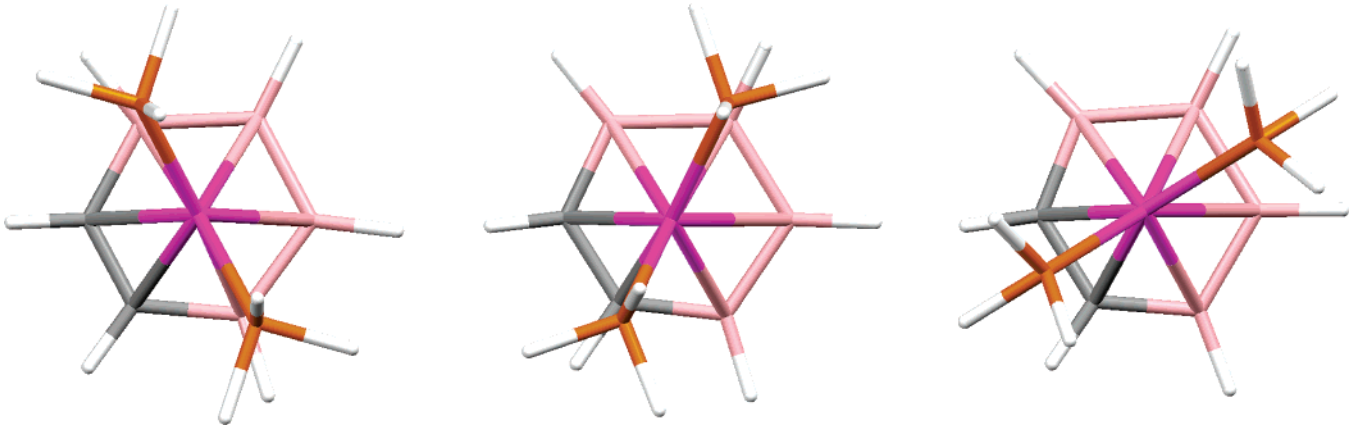

Figure 8. Computed [B3LYP/6-31G(d,p); Pt, SDD; P, SDD+d] conformations of $[(PH_3)_2Pt(C_2B_4H_6\text{-}1,2)]^{2-}$: (Left) Minimum energy. (Center) +0.68 kcal mol^{-1}. (Right) +4.4 kcal mol^{-1}.

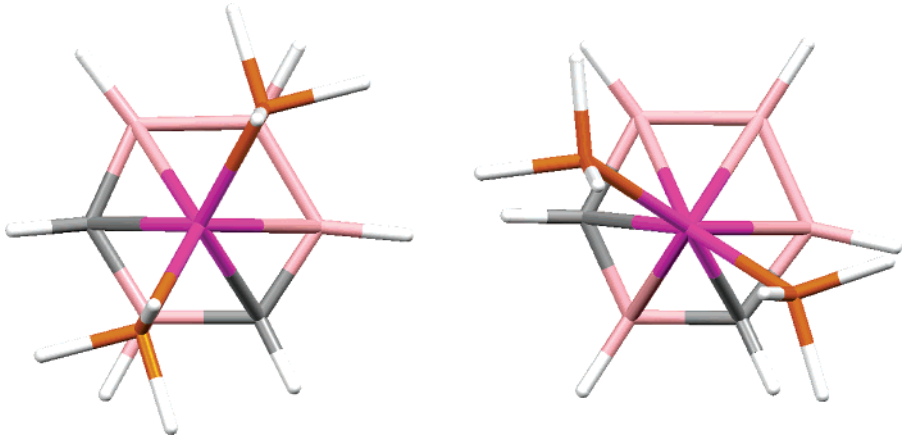

Figure 9. Computed [B3LYP/6-31G(d,p); Pt, SDD; P, SDD+d] conformations of $[(PH_3)_2Pt(C_2B_4H_6\text{-}1,3)]^{2-}$: (Left) Minimum energy. (Right) +19.1 kcal mol^{-1}.

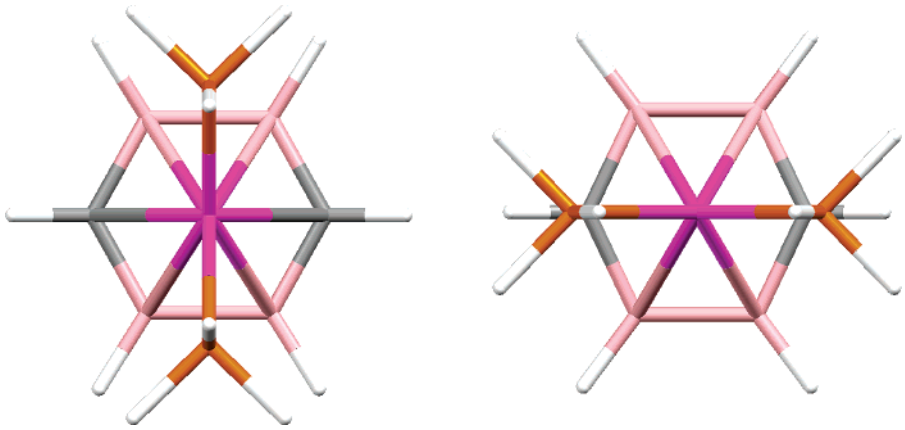

Figure 10. Computed [B3LYP/6-31G(d,p); Pt, SDD; P, SDD+d] conformations of $[(PH_3)_2Pt(C_2B_4H_6\text{-}1,4)]^{2-}$: (Left) Minimum energy. (Right) +22.0 kcal mol^{-1}.

geometry of this model compound corresponds to $\theta = 120°$ in 4,1,6-MC_2B_{10} metallacarboranes, in broad general agreement with experimental θ values of 148.7° (compound **3**), 134.6° and 136.7° (compound **4**), and 115.1° (compound **5**).

There are two mirror planes of symmetry perpendicular to the C_2B_4-1,4 heteroarene ring (the analogue of carborane type **V**), rendering the descriptors || and ⊥ inappropriate and conferring potential C_{2v} symmetry on the $[(PH_3)_2PtC_2B_4H_6]^{2-}$ ion. In C_{2v} symmetry the minimum structure (Figure 10, left) has PtP_2 and PtC_2 planes orthogonal and lies 22.0 kcal mol^{-1} below its rotamer in which the $\{(PH_3)_2Pt\}$ fragment eclipses the C atoms (Figure 10, right). Again, the latter does not correspond to a local minimum, having two imaginary frequencies, one corresponding to $\{Pt(PH_3)_2\}$ rotation and the other to PH_3 rotation. In C_1 symmetry exactly the same minimum as that shown in Figure 10 (left) is found, with the form of Figure 10 (right) collapsing to this by simple $\{Pt(PH_3)_2\}$ rotation. The minimum structure corresponds to $\theta = 90°$ in metallacarboranes

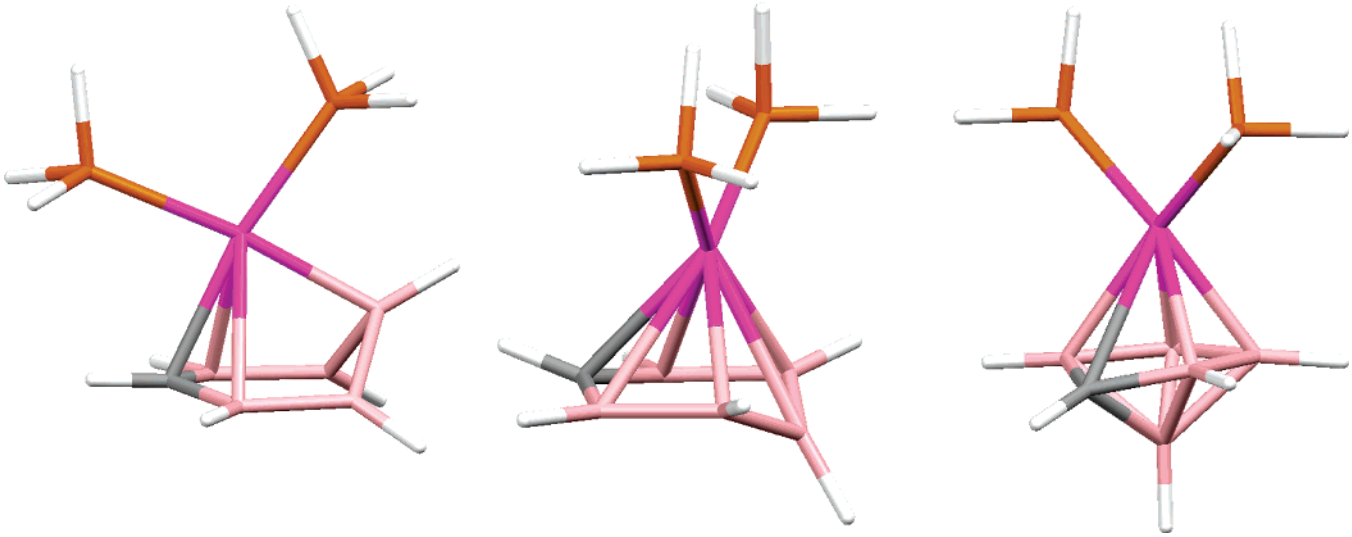

Figure 11. Results of attempted optimization [B3LYP/6-31G(d,p); Pt, SDD; P, SDD+d] of $[(PH_3)_2PtCB_5H_6]^{3-}$: (Left and center) with C_s symmetry imposed. (Right) with no imposed symmetry. Although the form on the right is ~50 kcal mol^{-1} more stable than the others, the original structure with a CB_5 metallabonded ring has collapsed to give a distorted closo 7-vertex platinacarborane with only a CB_4 metallabonded ring.

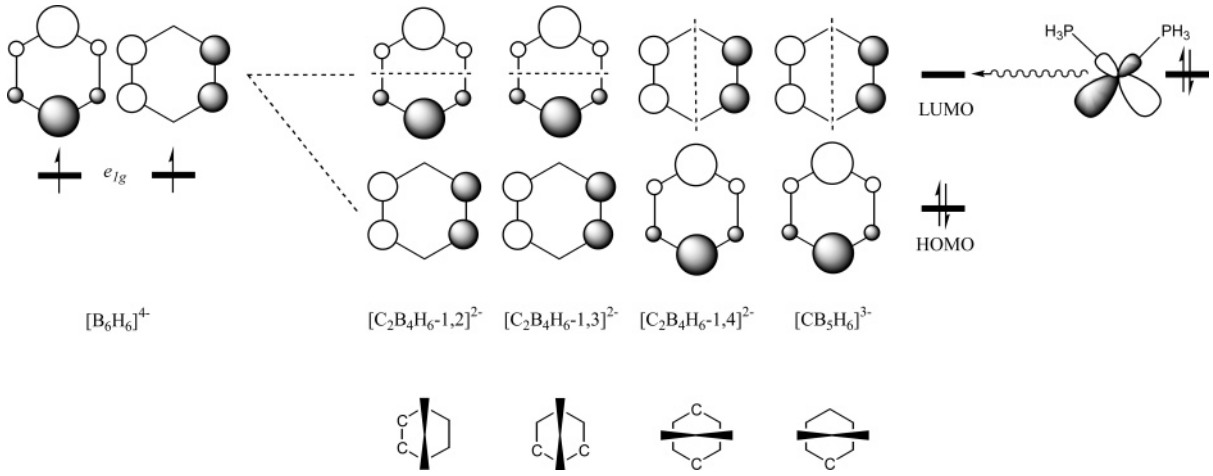

Figure 12. Qualitative representation of the splitting of the e_{1g} pair of MOs of $[B_6H_6]^{4-}$ on carbon atom substitution, leading to (lower part) predicted conformations for the three isomers of $[(PH_3)_2PtC_2B_4H_6]^{2-}$ and for $[(PH_3)_2PtCB_5H_6]^{3-}$.

incorporating the ligand type **V**, in excellent agreement with measured θ values of 87.7°, 89.4°, and 104.2° in compounds **6**, **7**, and **8**, respectively.

Finally, we attempted to optimize || and ⊥ forms of $[(PH_3)_2PtCB_5H_6]^{3-}$ in which the $\{(PH_3)_2Pt\}$ fragment is bonded to a CB_5 ring, the analogue of carborane type **VI**. However, this species, a model for both 4,1,8- and 4,1,12-*M*C_2B_{10} metallacarboranes (the latter represented experimentally by **9**), did not optimize as expected. If C_s symmetry is imposed, two structures are found, one || and the other ⊥, but neither is a minimum, each having two imaginary frequencies. The former (Figure 11, left) has the B atom opposite C substantially displaced out of the ring toward Pt, whereas in the latter (Figure 11, center) the CB_5 ring has a chair conformation with the B opposite C bent away from Pt and an unrealistic B−H vector. In C_1 symmetry, a minimum ***is*** found (~50 kcal mol^{-1} below the two former structures), but this structure has collapsed from a nido species with a CB_5 metallabonded ring into a distorted closo 7-vertex platinacarborane in which the metal is attached to only a CB_4 ring. This form (Figure 11, right) has effective C_s symmetry but cannot be accessed without removal of the symmetry constraint.

A qualitative understanding of the $[(PH_3)_2PtC_2B_4H_6]^{2-}$ conformations can be gained by considering how the degeneracy of the e_{1g} pair of π MOs of $[B_6H_6]^{4-}$ is lifted upon carbon substitution (Figure 12). Since C is more electronegative than B, that orbital with the greater coefficient on C will be preferentially stabilized, becoming the HOMO of $[C_2B_4H_6]^{2-}$ (or $[CB_5H_6]^{3-}$). Conversely, the component of the e_{1g} pair with the smaller coefficient on C will form the LUMO of the heteroarene. By analogy with the previous work[14] on icosahedral platinacarboranes, we would expect the conformation to be set by the metal HOMO/heteroarene LUMO interaction, leading to the predicted conformations of $[(PH_3)_2PtC_2B_4H_6]^{2-}$ shown in Figure 12, all of which are confirmed by calculation and supported by the crystallographic work on compounds **1**−**8**. This analysis also predicts a ⊥ conformation for $[(PH_3)_2PtCB_5H_6]^{3-}$. Although this model compound was not stable under optimiza-

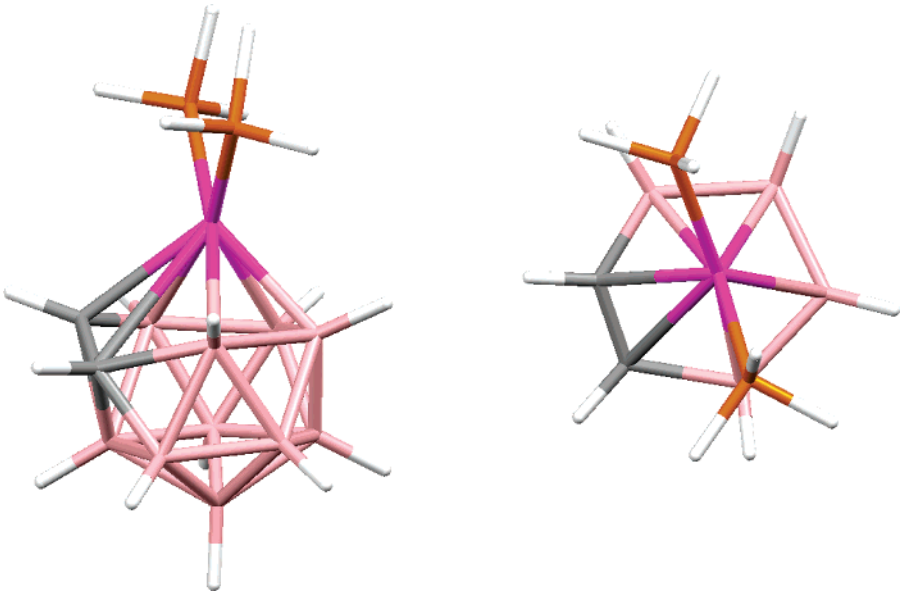

Figure 13. Optimized structure [B3LYP/6-31G(d,p); Pt, SDD; P, SDD+d] of 4,4-$(PH_3)_2$-4,1,2-*closo*-$PtC_2B_{10}H_{12}$ in C_1 symmetry: (Left) Perspective view. (Right;) View showing the conformation. $\theta = 68.4°$.

Table 6. Comparison of Selected Molecular Parameters (Å, deg) in (Theoretical) 4,4-$(PH_3)_2$-4,1,2-*closo*-$PtC_2B_{10}H_{12}$ and (Experimental) 1,2-$(CH_2)_3$-4,4-$(PMe_2Ph)_2$-4,1,2-*closo*-$PtC_2B_{10}H_{10}$, **1**

	$(PH_3)_2PtC_2B_{10}H_{12}$	**1**[a]
Pt4−C1	2.511	2.381(8)
Pt4−C2	2.906	2.626(8)
Pt4−B3	2.341	2.322(8)
Pt4−B6	2.312	2.310(7)
Pt4−B7	2.307	2.305(7)
Pt4−B10	2.253	2.265(7)
C2−B5	1.797	2.055(12)
Pt4−P1	2.335	2.3046(18)
Pt4−P2	2.353	2.3001(17)
P1−Pt4−P2	98.2	96.07(6)
θ	68.0	60.8

[a] Data taken from ref 8.

tion, such a ⊥ conformation is displayed by the analogous real compound **9**.

While we have noted good general agreement between the experimental conformations in compounds **1**−**8** and those predicted for the appropriate models with C_2B_4 heteroarene ligands, we recognize that these simple models are somewhat inappropriate in that, in the real systems, the two cage C atoms are not equivalent, one being of degree-four and the other degree-five. We have therefore extended the computational work to include optimizations of the 4,1,2-, 4,1,6-, and 4,1,10- isomers of the model 13-vertex metallacarborane, $(PH_3)_2PtC_2B_{10}H_{12}$, more closely to mimic the real systems. We have also optimized 4,4-$(PH_3)_2$-4,1,12-*closo*-$PtC_2B_{10}H_{12}$, which could not satisfactorily be modeled by $[(PH_3)_2PtCB_5H_6]^{3-}$.

Figure 13 shows the structure optimized in C_1 symmetry for 4,4-$(PH_3)_2$-4,1,2-*closo*-$PtC_2B_{10}H_{12}$, and Table 6 provides a comparison of key molecular parameters for this optimized structure and for that of the analogous compound 1,2-$(CH_2)_3$-4,4-$(PMe_2Ph)_2$-4,1,2-*closo*-$PtC_2B_{10}H_{10}$, **1**.[8] There is generally good agreement between calculated and found molecular structures, except that Pt4−C1 is somewhat overestimated in the calculation, by ∼0.13 Å, and more seriously, C2−B5 is ∼0.26 Å too short and Pt4−C2 is ∼0.28 Å too long, in the computed model. Thus, while the experimental structure shows

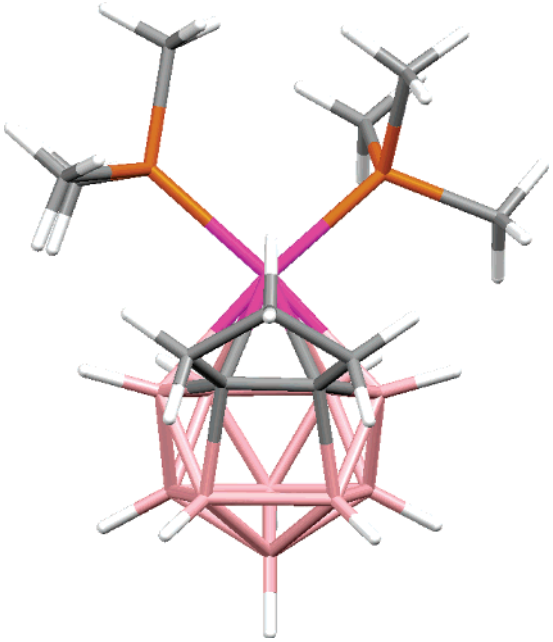

Figure 14. Henicosahedral transition state computed [B3LYP/6-31G(d,p); Pt, SDD; P, SDD+d] for 1,2-$(CH_2)_3$-4,4-$(PMe_3)_2$-4,1,2-*closo*-$PtC_2B_{10}H_{10}$.

a clear distortion toward henicosahedron **II**, the computed structure is more like docosahedron **I**, albeit with a very extended Pt4−C2 connectivity. Nevertheless, the computed conformation (right side of Figure 13), with $\theta = 68.4°$, is in reasonable agreement with that found, $\theta = 61.1°$ (Figure 1).

Seeking further to understand these differences between computed and experimental results, we have also performed calculations on a much more representative species, 1,2-$(CH_2)_3$-4,4-$(PMe_3)_2$-4,1,2-*closo*-$PtC_2B_{10}H_{10}$, in which the tether is included and a more realistic phosphine is used. In C_1 symmetry this optimized with much the same cage structure as that found for the simplified species, 4,4-$(PH_3)_2$-4,1,2-*closo*-$PtC_2B_{10}H_{12}$, i.e. with long Pt4−C2 (2.98 Å) and short C2−B5 (1.83 Å). However, in separate calculations we also noticed that artificially lengthening C2−B5 and concomitantly shortening Pt4−C2 to

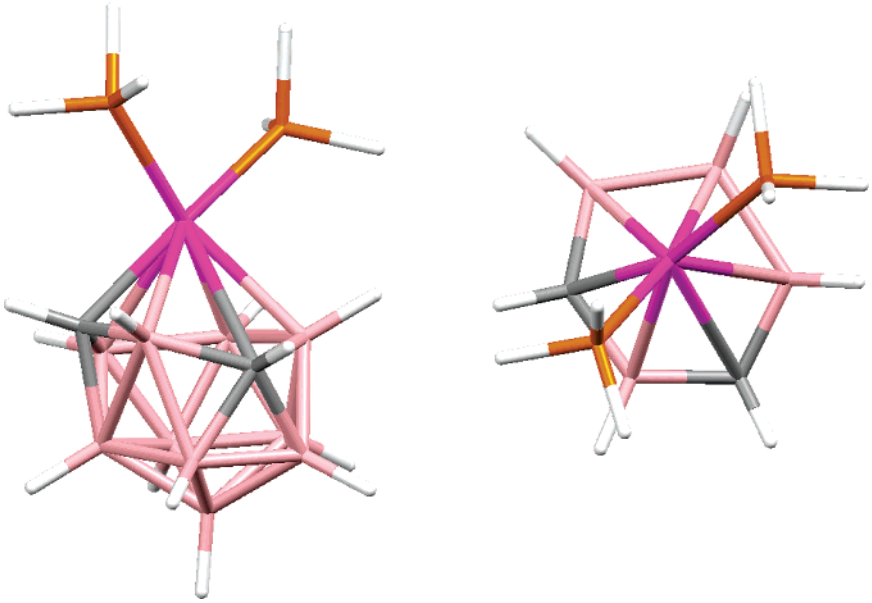

Figure 15. Optimized structure [B3LYP/6-31G(d,p); Pt, SDD; P, SDD+d] of 4,4-$(PH_3)_2$-4,1,6-*closo*-$PtC_2B_{10}H_{12}$ in C_1 symmetry: (Left) Perspective view. (Right) View showing the conformation. $\theta = 141.1°$.

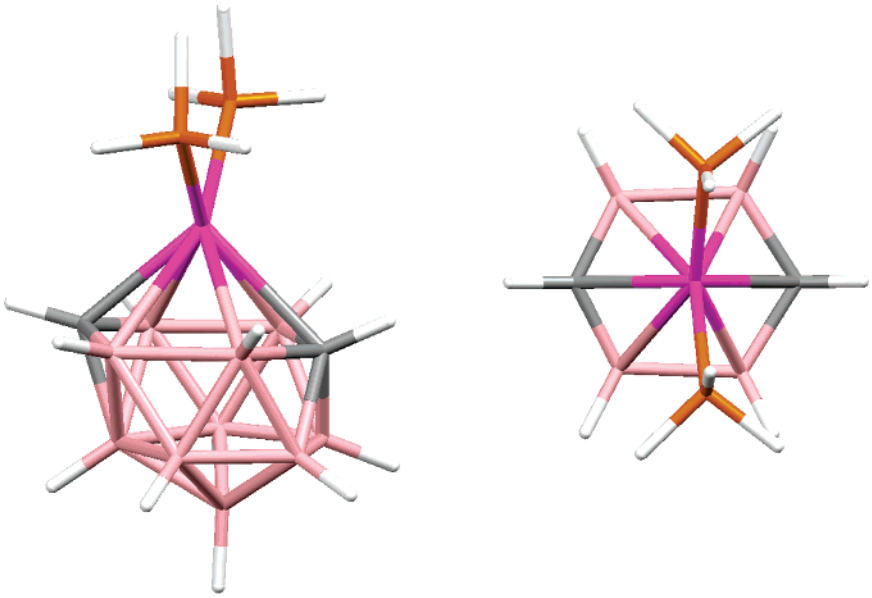

Figure 16. Optimized structure [B3LYP/6-31G(d,p); Pt, SDD; P, SDD+d] of 4,4-$(PH_3)_2$-4,1,10-*closo*-$PtC_2B_{10}H_{12}$ in C_s symmetry: (Left) Perspective view. (Right) View showing the conformation. $\theta = 90.0°$ by symmetry.

values typical of those observed experimentally[8] results in only a marginally less stable molecule, perhaps suggesting that the observed structure is influenced by solid-state effects to some extent. Moreover, a relatively soft potential surface for this deformation is entirely consistent with the facile diamond−trapezium−diamond process we have previously proposed[8] to account for the fluxionality of compound **1** (and its Nidppe analogue) in solution, as evidenced by ^{11}B and ^{31}P NMR spectroscopy. In this process the docosahedral ground-state structure transforms to the C_s symmetric henicosahedron via, predominantly, C2−B5 extension and Pt4−C2 contraction. The henicosahedron could either collapse back to the original docosahedron or to its mirror image in which C1−B9 shortened and Pt4−C1 lengthened. Since we could not arrest the fluxionality of **1** at low temperature we surmised that the activation energy for the process was unlikely to be greater than ∼10 kcal mol^{-1}.[29] For 1,2-$(CH_2)_3$-4,4-$(PMe_3)_2$-4,1,2-*closo*-$PtC_2B_{10}H_{10}$ a henicosahedral transition state was subsequently located 8.3 kcal mol^{-1} above the ground-state structure, entirely in keeping with this suggestion. This transition state is shown in Figure 14. It has nearly perfect C_s cage symmetry, broken only for the molecule as a whole by a staggered arrangement of the {$Pt(PMe_3)_2$} unit. Pt4−C2 (= Pt4−C1) is 2.52 Å and C2−B5 (= C1−B9) is 2.46 Å. Reassuringly, a similar henicosahedral transition state was also located for the simplified model compound, 4,4-$(PH_3)_2$-4,1,2-*closo*-$PtC_2B_{10}H_{12}$, 7.5 kcal mol^{-1}

(29) Abel, E. W.; Bhargava, J. K.; Orrell, K. G. *Prog. Inorg. Chem.* **1984**, *32*, 1.
(30) *The United Kingdom Chemical Database Service*; Fletcher, D. A.; McMeeking, R. F.; Parkin, D. *J. Chem. Inf. Comput. Sci.* **1996**, *36*, 746.

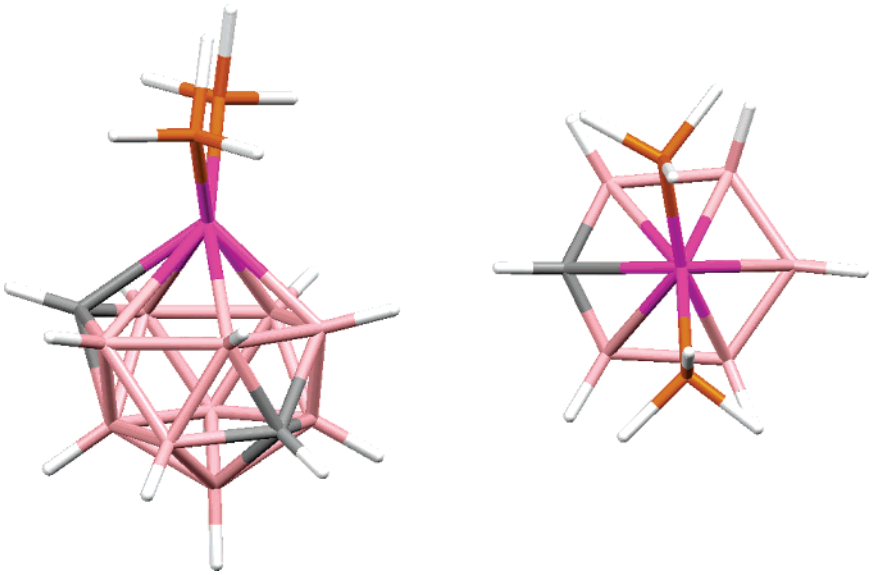

Figure 17. Optimized structure [B3LYP/6-31G(d,p); Pt, SDD; P, SDD+d] of 4,4-$(PH_3)_2$-4,1,12-*closo*-$PtC_2B_{10}H_{12}$ in C_1 symmetry: (Left) Perspective view. (Right) View showing the conformation. $\theta = 84.4°$.

Table 7. Comparison of Selected Molecular Parameters (Å, deg) in (Theoretical) 4,4-$(PH_3)_2$-4,1,6-*closo*-$PtC_2B_{10}H_{12}$ and (Experimental) 4,4-$(PMe_2Ph)_2$-4,1,6-*closo*-$PtC_2B_{10}H_{12}$, **3**

	$(PH_3)_2PtC_2B_{10}H_{12}$	**3**
Pt4−C1	2.180	2.1652(12)
Pt4−B2	2.499	2.4438(15)
Pt4−B3	2.445	2.3961(14)
Pt4−C6	2.956	2.8131(13)
Pt4−B7	2.244	2.2631(14)
Pt4−B10	2.475	2.3692(14)
Pt4−P1	2.300	2.2710(3)
Pt4−P2	2.378	2.3129(4)
P1−Pt4−P2	97.25	92.363(14)
θ	141.3	148.4

above the ground-state structure, implying that, at least in terms of the activation barrier, these simplified models represent appropriate approximations.

The structure calculated (in C_1 symmetry) for 4,4-$(PH_3)_2$-4,1,6-*closo*-$PtC_2B_{10}H_{12}$ is shown in Figure 15 and is in good agreement with that already described for compound **3**. Table 7 compares key molecular parameters. The greatest discrepancies are in Pt4−C6 and Pt4−B10 separations, too long in the calculations by ∼0.15 and 0.10 Å, respectively. Nevertheless, the very long Pt−C6 distance and severe buckling of the C_2B_4 carborane ligand face are both faithfully reproduced in the calculation, which also successfully predicts (in the correct sense) unequal Pt−P distances. The calculated ($\theta = 141.1°$) and observed ($\theta = 148.7°$) conformations also agree well, and it is particularly noteworthy that the conformation of this platinacarborane is much better reproduced in the model using a C_2B_{10} ligand rather than the simplified (heteroarene) C_2B_4 ligand.

In Figure 16 are perspective and plan views of the structure of 4,4-$(PH_3)_2$-4,1,10-*closo*-$PtC_2B_{10}H_{12}$ optimized in C_s symmetry, while Table 8 lists selected molecular parameters. The appropriate comparison here would be with the structure determined for **6**, but unfortunately, as noted above, this suffers from crystallographic disorder which masks subtle variations within the cage. Thus, for example, while the computational study predicts different Pt−C distances (Pt4−C1 2.291 Å, Pt4−C10 2.484 Å), in the diffraction study C1 and C10 are disordered about a crystallographic C_2 axis, and a single, average Pt−C distance is measured, 2.357(2) Å. Nevertheless, the overall comparison between experimental and computational structures is clearly very good. In the crystallographic study $\theta = 87.7°$, while in the computational study it is required to be precisely 90.0° by the C_s symmetry imposed.

Table 8. Selected Molecular Parameters (Å, deg) for the C_s Symmetric Optimized Structure of 4,4-$(PH_3)_2$-4,1,10-*closo*-$PtC_2B_{10}H_{12}$

C1−B2	1.533	Pt4−B6	2.344	B9−B11	1.770
C1−Pt4	2.315	Pt4−C10	2.497	B9−B12	1.750
C1−B5	1.783	B5−B9	1.897	C10−B12	1.680
B2−Pt4	2.412	B5−B11	1.766	B11−B12	1.790
B2−B5	2.022	B6−B9	1.770	B12−B13	1.760
B2−B6	1.927	B6−C10	1.682	Pt4−P1	2.334
B2−B9	1.793	B6−B12	1.773	P1−Pt4−P1A	97.28

Table 9. Selected Molecular Parameters (Å, deg) for the C_1 Symmetric Optimized Structure of 4,4-$(PH_3)_2$-4,1,12-*closo*-$PtC_2B_{10}H_{12}$

C1−B2	1.529	Pt4−B6	2.250	B8−B11	1.746
C1−B3	1.539	Pt4−B7	2.297	B8−B13	1.756
C1−Pt4	2.384	Pt4−B10	2.301	B9−B11	1.762
C1−B5	1.784	B5−B8	1.901	B9−C12	1.683
B2−Pt4	2.500	B5−B9	1.886	B10−C12	1.704
B2−B5	2.007	B5−B11	1.768	B10−B13	1.770
B2−B6	1.920	B6−B9	1.770	B11−C12	1.722
B2−B9	1.770	B6−B10	1.847	B11−B13	1.786
B3−Pt4	2.451	B6−C12	1.679	C12−B13	1.692
B3−B5	2.015	B7−B8	1.784	Pt4−P1[a]	2.338
B3−B7	1.930	B7−B10	1.794	Pt4−P2[a]	2.341
B3−B8	1.783	B7−B13	1.752	P1−Pt4−P2	95.25

[a] P1 trans to B3−B7 and P2 trans to B2−B6, as in compound **9**.

Figure 17 shows the structure optimized for 4,4-$(PH_3)_2$-4,1,12-*closo*-$PtC_2B_{10}H_{12}$, and Table 9 lists important derived molecular parameters. Although we do not have an experimental 4,1,12-*closo*-PtC_2B_{10} compound with which to compare this computational result (the obvious precursor, compound **6**, is relatively unstable and does not survive even gentle thermolysis), it is encouraging that the main features of the only two 4,1,12-MC_2B_{10} species to have been crystallographically characterized,

4-Cp*-4,1,12-*closo*-$CoC_2B_{10}H_{12}$[10k] (Cp* = η-C_5Me_5) and 4,4-dppe-4,1,12-*closo*-$NiC_2B_{10}H_{12}$, **9**,[6a] viz. long B2−B5, B3−B5, and B5−B9 distances, are reproduced by the calculation. Moreover, the calculated θ value, 84.4°, is in excellent agreement with that measured for **9**, 90.0°.

Conclusions

Recent developments in supraicosahedral metallacarborane chemistry have allowed access to homologous series of compounds with four different types of six-atom faces presented to the metal fragment; including the three new compounds reported herein, we now have a total of nine crystallographically characterized examples of species with $\{ML_2\}$ fragments bound to these six-atom faces. In these species clear patterns are visible in the conformations of the $\{ML_2\}$ fragments with respect to the carborane ligand.

Initially we explored these conformations for C_2B_4 carborane faces by DFT calculations on the model compounds $[(PH_3)_2PtC_2B_4H_6]^{2-}$ and successfully rationalized the results by qualitative MO arguments. Unfortunately, analogous calculations on $[(PH_3)_2PtCB_5H_6]^{3-}$ as a model compound with a CB_5 ligand face were unsuccessful. However, further calculations on the polyhedral model compounds $(PH_3)_2PtC_2B_{10}H_{12}$ successfully reproduced the observed conformations for all four types of carborane ligand.

In some cases the calculations led to apparent overestimation of Pt−C distances, and in investigating this for the realistic model compound, 1,2-$(CH_2)_3$-4,4-$(PMe_3)_2$-4,1,2-*closo*-$PtC_2B_{10}H_{10}$, we were able to compute a low activation energy for interconversion of docosahedral enantiomers, consistent with our inability to arrest the fluxionality of 1,2-$(CH_2)_3$-4,4-$(PMe_2Ph)_2$-4,1,2-*closo*-$PtC_2B_{10}H_{10}$. Calculations on $(PH_3)_2PtC_2B_{10}H_{12}$ also allowed the structure of the experimentally unavailable 4,1,12-PtC_2B_{10} cluster to be explored and proved superior to experiment in the case of the severely crystallographically disordered 4,1,10-PtC_2B_{10} species.

Acknowledgment. We thank the EPSRC (D.E., S.E.), the Carnegie Trust (R.D.McI.), and the Robert A. Welch Foundation (B.E.H., T.D.McG.; Grant AA-0006) for support. At Heriot-Watt we thank Dr. A. S. F. Boyd for NMR spectra, Mr. G. Smith for mass spectra, Ms. C. Graham for elemental analysis, and we acknowledge provision of the diffractometer from EPSRC Grant GR/R99065. At Baylor the diffractometer was purchased with funds from the National Science Foundation Major Research Instrumentation Programme (Grant CHE-0321214). We acknowledge use of the EPSRC Chemical Database Service at Daresbury.[30] V.S. is the recipient of a Socrates scholarship from the Philipps-Universität Marburg, Germany.

Supporting Information Available: Full details of the crystallographic analyses of **3**, **6**, and **8**·$^1/_2CH_2Cl_2$ as a CIF; Cartesian coordinates of all model compounds shown in Figures or otherwise discussed in the text along with complete ref 23 as a text file. This material is available free of charge via the Internet at http://pubs.acs.org

JA067698M